CrossMark

Elucidating the evolution of the current-voltage characteristics of planar organometal halide perovskite solar cells to an S-shape at low temperature

Fei Xu [a,b,*], Jiabin Zhu [a], Runan Cao [a], Sheng Ge [c], Wenzhen Wang [c], Haitao Xu [c], Run Xu [c], Yanglin Wu [c], Ming Gao [a], Zhongquan Ma [a], Feng Hong [a], Zuimin Jiang [b]

[a] SHU-SolarE R&D Lab, Department of Physics, College of Sciences, Shanghai Key Laboratory of High Temperature Superconductors, Shanghai University, Shanghai 200444, China
[b] State Key Laboratory of Surface Physics and Department of Physics, Key Laboratory of Micro and Nano Photonic Structure (Ministry of Education), Fudan University, Shanghai 200433, China
[c] Department of Electronic Information Materials, School of Materials Science and Engineering, Shanghai University, Shanghai 200444, China

ARTICLE INFO

ABSTRACT

The temperature dependence of initial transient current-voltage (I-V) characteristic of planar perovskite solar cell by one-step solution process is investigated. An S-shaped I-V characteristic emerges in response to low temperature and the photovoltaic parameters drop dramatically. This is mainly attributed to the increasing amount of negative charges accumulating in the TiO$_2$/CH$_3$NH$_3$PbI$_3$ interface region and the reduced built-in field separating the photo-generated carriers in the absorber layer. The influence of negative charge accumulation can be represented by two extra diodes that are in series with a conventional solar cell circuit model at low temperature whereas it acts as a resistor with low resistivity above room temperature. These findings help to understand the charge transport mechanism in perovskite solar cells.

1. Introduction

Recently, a novel organometal halide perovskite (CH$_3$NH$_3$PbI$_3$), as a promising absorption material, has attracted much attention for its outstanding photovoltaic performance. The optical bandgap of this material is 1.61 eV and its absorption coefficient 1.5×10^4 cm^{-1} at 540 nm, which is an order of magnitude higher than that of dye N719 in dye-sensitized solar cell (DSSC) [1,2]. The power conversion efficiency (PCE) of perovskite solar cell has been increased rapidly from 3.81% to 22.1% in about seven years under the standard test condition (STC) (i.e. 298 K, simulated one-sun illumination (AM 1.5G, 100 mW/cm^2)) [3,4].

However, it is noteworthy from those previously reported that a dramatic decrease in photovoltaic performance from perovskite solar cell has been found at low temperature regardless of whether perovskite solar cell is planar or mesoporous. For instance, the

short-circuit current (J$_{SC}$), fill factor (FF) and PCE of the mesoporous perovskite solar cell decreases sharply when the operating temperature goes down to 80 K [5]. For another instance, the PCE of planar perovskite solar cell reduces from approximate13–2% with decreasing the operating temperature from 298 K to 233 K [6]. The temperature-dependent I-V characteristic is different from those from most solar cells, such as DSSC and blended heterojunction organic solar cell [7,8]. In both cases, it should be noted that FF is also reduced with the decreasing photovoltaic performance. FF decreases gradually from 0.72 to 0.16 in the former situation, indicating a general trend that a convex I-V shape turns into a concave I-V shape (S-shaped I-V) [9]. The interface effect is generally regarded as the primary cause of S-shaped I-V [10,11]. From this point of view, the interface effect has a fairly underlying impact on the photovoltaic performance degradation at low temperature.

In this paper, the temperature dependence of initial transient I-V characteristic of the planar perovskite solar cell is studied. We find that the initial state of perovskite solar cell shows an S-shaped I-V characteristic at the low temperature, meanwhile, the photovoltaic performance drops dramatically. This phenomenon is caused by the negative charge accumulation in the interface

* Corresponding author at: SHU-SolarE R&D Lab, Department of Physics, College of Sciences, Shanghai Key Laboratory of High Temperature Superconductors, Shanghai University, Shanghai 200444, China.
E-mail addresses: drfeixu@gmail.com, feixu@staff.shu.edu.cn (F. Xu), runxu@staff.shu.edu.cn (R. Xu).

region. A three diode circuit model, including the two extra diodes representing the trap states and ions (negatively charged Pb^{2+} vacancies), is employed to fit the measured I-V curve. These findings may contribute to understanding of carrier transport mechanism in perovskite solar cell.

2. Experimental details

The planar perovskite solar cell was fabricated by one-step solution process. Firstly, the fluorine-doped thin oxide (FTO) glass substrates (HeptaChroma) were cleaned ultrasonically in ethanol, acetone and deionized water, respectively. To prepare the TiO_2 precursor solution, 700 μl tetraisopropyl titanate (Sigma) was added into 5 ml ethyl alcohol (solution A). Then 70 μl HCl (2 M) was added the into equal volume ethyl alcohol (solution B). The solution B was dripped into solution A slowly under vigorous stirring at room temperature. The TiO_2 precursor solution was aged for 24 h. A compact TiO_2 layer was deposited on FTO by spin-coating, followed by annealing at 773 K for 30 min. CH_3NH_3I was synthesized with CH_3NH_2 and HI in equimolar ratio. 57% aqueous hydroiodicacid (Sigma) was added into 33% methylamine ethanol solution (Sinopahrm) at 273 K. The resulting solution was carried out by rotary evaporation three times and the CH_3NH_3I powder was dried for 12 h in vacuum at 333 K. CH_3NH_3I and $PbCl_2$ (Sigma) powder were dissolved in the dimethyl formamide (DMF) in the mole ratio of 3:1. The $CH_3NH_3PbI_3$ precursor was annealed at 373 K for 90 min after dripping on TiO_2 through spin-coating. The hole-transporting material (HTM) precursor solution contained 0.170 M 2,2′,7,7′-tetrakis-(N,N-di-p-methoxyphenyl-amine)$-$9,9′-spirobifluorene (Spiro-OMeTAD), 0.198 M 34 μl 4-tert-butylpyridine (TBP), 0.064 M bis (trifluoromethane) sulfonimide lithium salt (Li-TFSI) dissolved in the mixed solvent of chlorobenzene and acetonitrile (1:0.1 v/v). The HTM layer was dried for 12 h after spin-coating. The fabrication of perovskite and HTM thin film was in N_2-filled glovebox. Finally, Au electrode was deposited by thermal evaporation. The photovoltaic properties of planar perovskite solar cell were characterized by I–V measurements either in the dark or under AM1.5 G (100 mW/cm^2) illumination at 298 K by a source meter (Keithley Series 2400) and a solar simulator (Sciencetech SS1k). For our typical planar perovskite solar cell, the PCE measured at room temperature under AM1.5 G illumination is attained to be 12.8%. The open circuit voltage (V_{oc}), short-circuit current (J_{sc}) and fill factor (FF) are 0.870 V, 20.8 mA/cm^2 and 0.71, respectively.

Characterization of the perovskite film and solar cell was carried out by X-ray photoelectron spectroscopy (XPS) (Thermo Scientific Escalab 250Xi), temperature-dependent absorbance spectroscopy (AS), temperature-dependent electroabsorption (EA), temperature-dependent current density-voltage (J-V) measurement, respectively. The XR6 monochromated X-ray source used Al Kα radiation with a photon energy of 1486.6 eV and an energy resolution of about 0.45 eV (Ag 3d5/2). For temperature-dependent measurements such as AS, EA and J-V, samples were carried out using a home-made integrated optoelectronic measurement system [12]. During the measurements, samples were kept in vacuum so that this could make sure that perovskite film and solar cell were unaffected by O_2, N_2 and H_2O from atmosphere. Samples were loaded into a cryostat chamber (CS202-x1) that was connected to a water cooled helium compressor (ARS-2HW). The operating temperature is varied from 200 K to 325 K. For AS and EA measurements, a monochromator 7ISW303 is used to split the halogen light into its component wavelengths. The light was collected by a Si detector for the 300 nm to 1100 nm spectral range. The signal was then fed into a lock-in amplifier (Stanford Research Systems Model SR 830) under the R and θ modes. For the light

reflection R measurement in EA spectrum [13], a chopper wheel was placed in front of the detector as the reference (33 Hz) to the lock-in amplifier. For the EA scan, an ac voltage (V_{ac}) was produced by a Gwinstek AFG-2225 arbitrary function generator and summed to a dc voltage (V_{dc}) before being applied to the gate electrode. The sine wave modulation with ac frequency 2 kHz was used as the reference to the lock-in amplifier and the voltage modulated transmission ΔR was measured. Light I-V curve was measured by Agilent E4980A. In order to investigate the initial transient state, the scan rate was set to 1.33 V/s, close to the system limit.

3. Results and discussion

Fig. 1(a) shows the cross sectional scanning electron microscopy (SEM) image and band diagram at equilibrium of the planar perovskite solar cell fabricated through one-step solution process. The perovskite solar cell consists of FTO layer (200 nm), TiO_2 compact layer (30 nm), perovskite absorber layer (300 nm) and HTM layer (500 nm), respectively. Due to the weak n-type conduction of perovskite thin film [14–16] fabricated by one-step solution process, the Fermi level in $CH_3NH_3PbI_3$ locates near the middle of energy band. Thus, the built-in field throughout the absorber layer originates from the difference of the work functions between TiO_2 and HTM as shown in Fig. 1(b).

Fig. 2(a) shows the initial transient I-V characteristics from reverse scan and corresponding photovoltaic parameters of the planar perovskite solar cell at the operating temperatures from 200 K to 325 K. Below 200 K, the perovskite solar cell shows no photovoltaic effect, due to phase transition from tetragonal to orthorhombic (not shown). An S-shaped I-V curve emerges when the operating temperature decreases. Furthermore, the V_{oc}, J_{sc} and FF
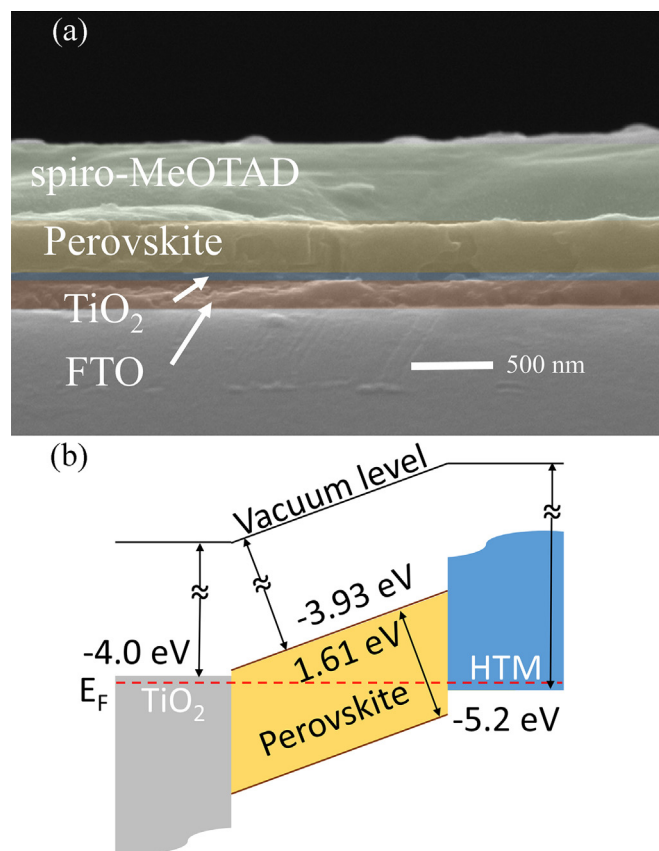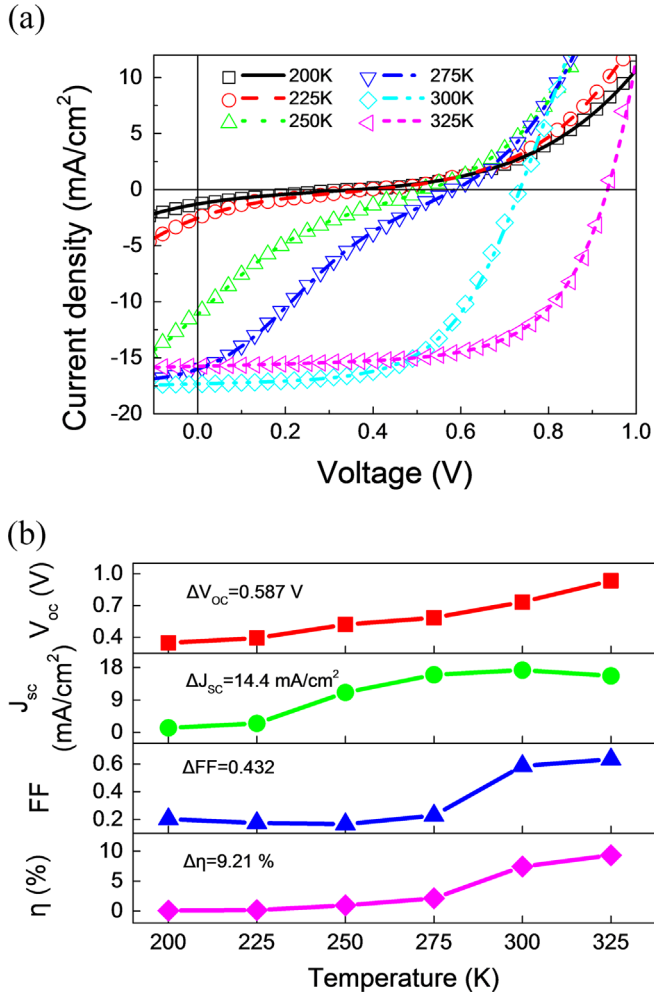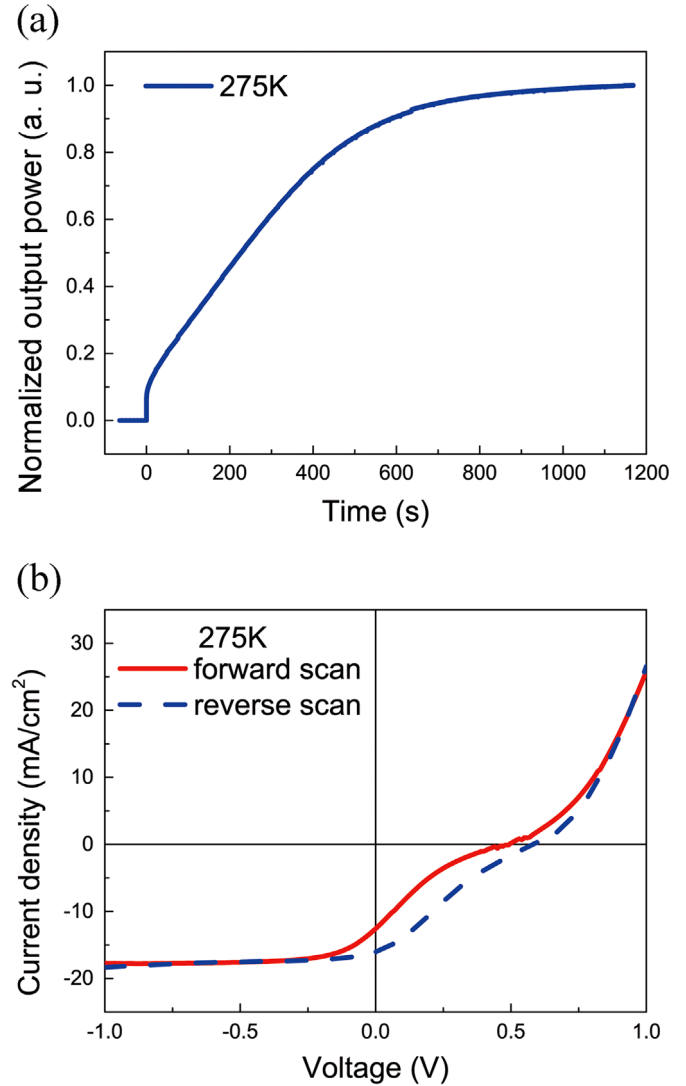

Fig. 1. (a) The cross sectional SEM image of perovskite solar cell, (b) Band diagram of perovskite solar cell at equilibrium.

(a)

(b)

Fig. 2. (a) I-V characteristics of perovskite solar cell measured at different operating temperatures varied from 200 K to 325 K. Dots refers to experimental data and lines correspond to fitting data through Eqs. ((1)–(3)). (b) Photovoltaic parameters extracted from the I-V curves at different temperatures. The difference of photovoltaic parameter measured at 200 K and 325 K are labeled on graph.

(a)

(b)

Fig. 3. (a) Variation of normalized output power at 275 K. The bias voltage is fixed at 0.5 V. (b) I-V curves measured in forward and reverse scan mode at 275 K.

decrease dramatically at low temperature, shown in Fig. 2(b). It is distinct from most solar cells, such as DSSC and blended heterojunction organic solar cell [7,8]. It should be pointed out that the I-V curves from reverse scan ($+1$ V to -1 V) and forward scan (-1 V to $+1$ V) show the same tendency as will be discussed in detail below.

To distinguish the initial and the steady state of perovskite solar cell, the time evolution measurement of output was carried out. We find that the perovskite solar cell needs a long activation time to reach the steady output state at low temperature. For an example, the time-dependence of normalized output power at 275 K is shown in Fig. 3(a). The bias voltage is fixed at 0.5 V, which is close to the maximum power point. The initial output power of perovskite solar cell is relatively low. After a long period of activation, the output power gradually increases to reach a relatively stable value. The data measured at other temperature point also show the similarity of time-dependent output power (not shown). It should be noted that the scan rate 1.33 V/s is fast enough to acquire the initial state of the perovskite solar cell. Fig. 3(b) shows the I-V curves measured in forward and reverse scan mode at 275 K. It indicates that the S-shaped I-V curves emerge at low temperature regardless of the hysteresis effect in perovskite solar cell. Both I-V curves measured in forward and reverse scan mode reflect the charge transport mechanism. However, the I-V curve

measured in forward scan mode usually underestimates the performance of perovskite solar cell. Therefore, the data measured in reverse scan mode is chosen for interpreting the charge transport mechanism.

To understand the temperature-dependent S-shaped I-V curve, an equivalent circuit model has been proposed as shown in Fig. 4 (a) [17]. It consists of three diodes D_1, D_2, and D_3. Diode D_1 represents the diffusion and recombination of carriers in the device. Diodes D_2 and D_3 represent the behavior of negative charge accumulating at trap states and ions, which mainly locate in the $TiO_2/CH_3NH_3PbI_3$ interface region [18–20], as observed by XPS in Fig. 5. Fig. 5 shows the concentration depth profiles of a planar perovskite solar cell as derived from the XPS spectra of Pb4f7 and I3d5 states. In the HTM/perovskite interface region, the I/Pb ratio is close to the 3: 1 stoichiometry of perovskite, implying almost nothing of ions (negatively charged Pb^{2+} vacancies or positively charged I^- vacancies) on that side. Across the perovskite layer, the ratio of I/Pb decreases to 2.6 and then increase to over 3. In the TiO_2/perovskite interface region, the ratio of I/Pb is around 3.3, indicating an accumulation of ions (negatively charged Pb^{2+} vacancies) there due to iodide ion migration [21,22]. This may result in the screening effect of the built-in field. That is, these two extra diodes D_2 and D_3 represent the effect of trap states and ions. If
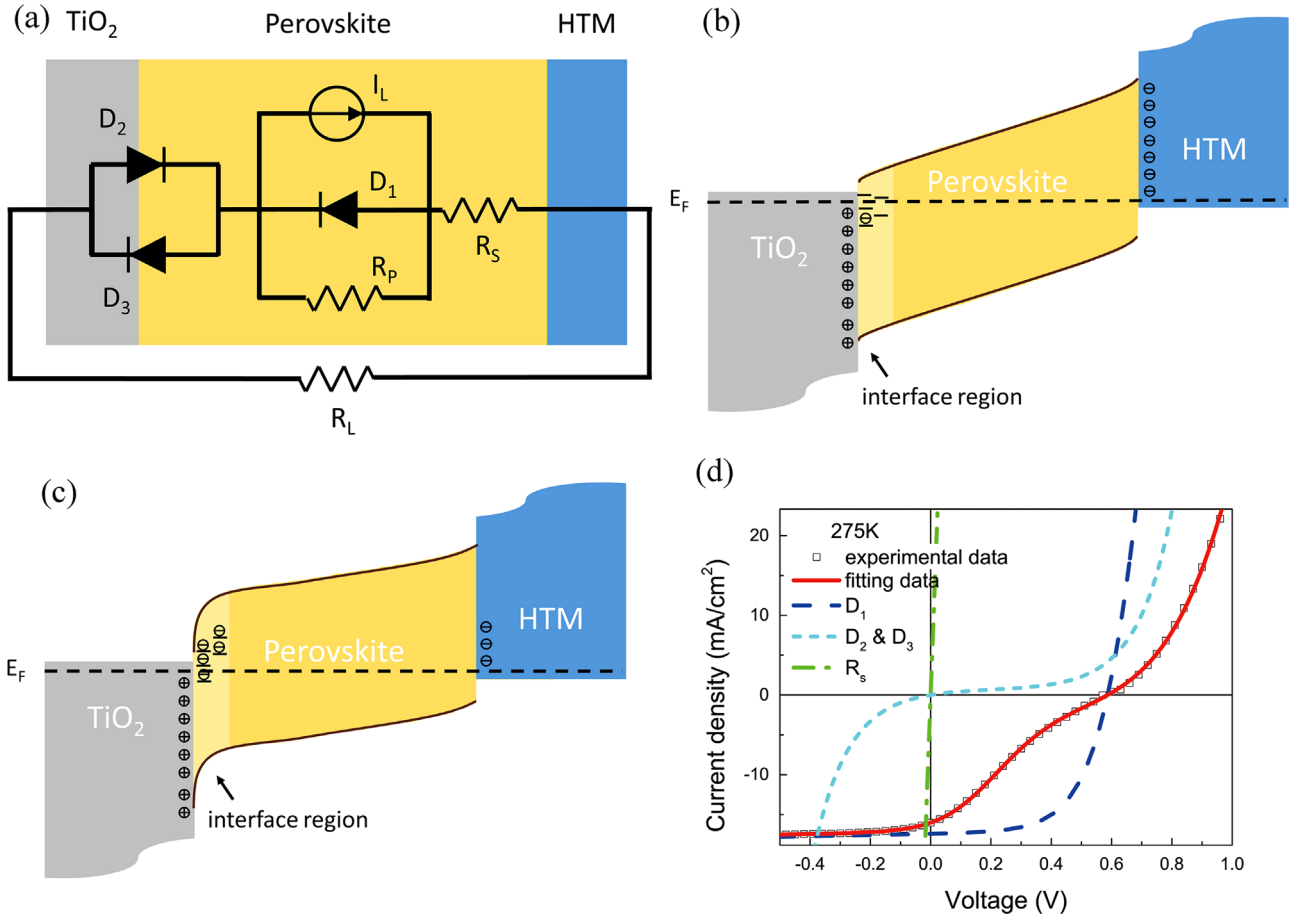
Fig. 4. (a) The equivalent circuit model employed to fit the I-V curve. Two opposite didoes in shunt connection are in series with a conventional solar cell equivalent circuit. (b) and (c) are the charge distribution and band diagram when the interface states are filled without and with negative charges. (d) S-shaped I-V curve measured at 275 K (open square). Fitting data (red line), diode D_1 (blue dash), diode D_2 and D_3 (cyan short dash) and series resistance (green dash dot). (For interpretation of the references to color in this figure legend, the reader is referred to the web version of this article.)
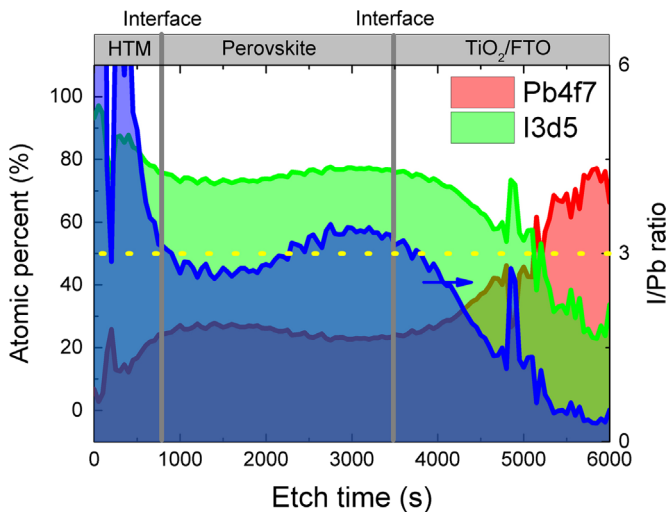
Fig. 5. Concentration depth profiles of a planar perovskite solar cell as derived from the XPS spectra of Pb4f7 and I3d5 states. The yellow dashed line indicates the stoichiometry of perovskite (3: 1). (For interpretation of the references to color in this figure legend, the reader is referred to the web version of this article.)

electrons are not trapped at interface states and less ions are piled, a strong built-in field is determined by the difference in work function of TiO_2 and HTM and by the band offsets, shown in Fig. 4 (b). When the interface states are negatively charged and the negatively charged ions are piled in the TiO_2/perovskite interface

region, the potential drop in the interface region is increased, thus it is reduced in the bulk, shown in Fig. 4(c). For $V < V_{oc}$ condition, D_2 works and D_3 is cut-off when photo-generated current flows through the D_2 and D_3 sub-circuit. The trapped electrons, negatively charged ions and the positive charges in TiO_2 (space charge) can be viewed as the charge in the diode D_2, which is positively biased and turn-on, corresponding to the short dash line in the third quadrant in Fig. 4(d). As the positive bias on the cell increases, the photo-generated current decreases and the potential drops on the D_2 decreases. D_2 turns into cutoff region. Therefore, the S-shape kink appears. When $V > V_{oc}$, the sign of space charge in TiO_2 and HTM changes. Diode D_1 is turn-on. However, at the $TiO_2/CH_3NH_3PbI_3$ interface region there is a potential drop due to the trapped electrons and ions. It can be viewed as the diode D_3, which is turn-on, corresponding to the short dash line in the first quadrant. Because of this additional potential drop, the onset voltage increases, comparing with the dash line.

According to the equivalent circuit model reported by García-Sánchez et. al, the S-shaped I-V curve can be fitted by the following equations as shown in Fig. 2(a) (lines) [17].

$$J = \frac{V_R}{R_S} \tag{1}$$

$$J = J_{01}\left(\exp\left(\frac{V_1}{n_1 kT}\right) - 1\right) + \frac{V_1}{R_{P1}} - J_L \tag{2}$$

Table 1
Parameters of diodes in equivalent circuit.

Temperature (K)	n_1	J_{01} (mA/cm^2)	n_2	J_{02} (mA/cm^2)	J_{03} (mA/cm^2)
200	7.6	4.6E-1	9.0	1.2E-1	3.4E-3
225	4.4	1.2E-1	7.5	1.7E-1	4.1E-3
250	3.5	1.5E-2	6.2	4.2E-1	1.6E-2
275	3.4	1.4E-2	4.8	6.9E-1	2.1E-2
300	3.7	7.7E-3	2.4	1.4E1	2.4E-2
325	3.9	2.7E-3	–	–	–

$$J = -J_{02}\left(\exp\left(-\frac{V_2}{n_2 kT}\right) - 1\right) + J_{03}\left(\exp\left(\frac{V_2}{n_3 kT}\right) - 1\right) \tag{3}$$

J is the current density flowing through the circuit. R_S and R_{p1} are the series and parallel resistances. J_{01}, J_{02} and J_{03} are the reverse saturation current densities of diode D_1, D_2 and D_3. n_1, n_2 and n_3 are the corresponding ideal factors of three diodes. V_R, V_1 and V_2 are the voltage drop on series resistance, diode D_1 and the sub-circuit containing diode D_2 and D_3. Table 1 lists the fitting parameters of the diodes D_1, D_2 and D_3 at the different operating temperatures. With decreasing temperature from room temperature, the reverse saturation current of diode D_1 (J_{01}) increases. Thus, more photo-generated carriers recombine in the device. Meanwhile, the S-shaped I-V curve emerges with the decreasing of J_{02} and J_{03} that represent the degree of curvature in the fourth quadrant [10]. Under this circumstances, some charges are prevented from transfer through interface region and the others recombines in the absorber layer [10,23]. This finally leads to the decreasing of V_{oc} and J_{sc}. Above room temperature, the absence of the fitting parameters of J_{02} and J_{03} suggests that the extra diodes D_2 and D_3 no longer influence the carrier transportation and they act as the resistors equivalently with low resistivity. This also means that all the photo-generated carriers can transport through the interface region. Thus, J_{01} decreases so that less recombination of photo-generated carriers takes place in the absorber layer.

It is noteworthy from recently reported by Maynard et. al [24] that the mobility of perovskite decrease with the decreasing temperature in methylammonium lead iodide perovskite solar cells. According to the theoretical analysis of the effect of mobility of perovskite layer on photovoltaic performance of perovskite solar cell using device simulation [25], the decreased mobility of perovskite would cause the decline of FF with decreasing operating temperature, as shown in Fig. 6. However, it is noted that the output power increase with the illumination time, as shown in Fig. 3(a). This implies that it is a dynamic process. In fact, mobility is not expected to be changed with illumination time. It is also noted that ion migration is considered as an origin of screening effect of built-in field during the continuous J_{SC} measurement [26]. Thus, the S-shaped I-V is not mainly caused by the decreased mobility. It is reported by Reenen et al. that the traps at the interface regions would cause the recombination of photo-generated carriers [27]. Moreover, the recombination rate is bias-dependent. They think that the recombination of photo-generated carriers becomes much more severe near the open-circuit voltage. In our model, the two extra diodes represent the effect of traps and ions. When the bias is close to the open-circuit voltage, the differential resistance of the sub-circuit including these two diodes is increased. This means that photo-current is consumed by the sub circuit. Therefore, the loss of photo-current causes the S-shaped I-V curve.

It should be noted that V_{oc} decreases sharply when the S-shaped I-V characteristic of planar perovskite solar cell emerges at the low temperature. This could be considered to be caused by
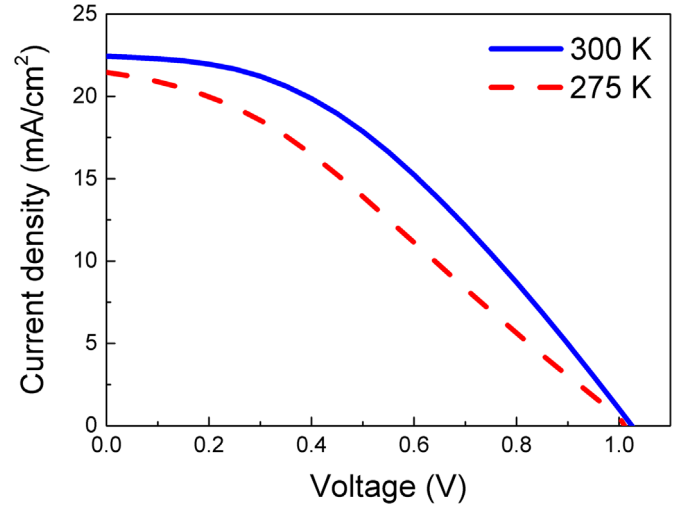

Fig. 6. Theoretical simulation of J-V curves of planar perovskite solar cell as a function of mobility.

the accumulation of negative charges at trap states and ions(negatively charged Pb^{2+} vacancies) in the TiO_2/perovskite interface region [11,28,29]. Fig. 7 shows the band diagram of planar perovskite solar cell at different operating temperatures under open circuit condition. Above room temperature, the supply of thermal energy is high and the built-in field determined by the Fermi level difference of TiO_2 and HTM is small. As a result, the trapped negative charges are ionized thermally and ions diffuse to the opposite direction. These trap states are introduced due to the decomposition of $CH_3NH_3PbI_3$ during annealing process [18,30]. And the small amount of ions pile in the interface region. The low number of trapped negative charges and ions in the interface region does not affect the built-in field distribution in Fig. 7(a). However, due to the lower supply of thermal energy at low temperature, fewer trapped negative charges can be ionized thermally and more ions pile in the interface regions due to drift [26]. Thus, the interface region is negative charged in Fig. 7(b). The charge distribution in the absorber layer is different from the former situation, so that V_{oc} decreases according to the following equation [31]

$$V_{oc} = \frac{E_g - \phi_e - \phi_h}{q} - \int_0^L F dx \tag{4}$$

where E_g is the energy bandgap of the absorber, Φ_e and Φ_h are the barriers at $TiO_2/CH_3NH_3PbI_3$ and $HTM/CH_3NH_3PbI_3$ interface, respectively. This is caused by the affinity difference between two materials. F represents the electric field in the absorber layer and L is the thickness of the absorber layer. More negative charge accumulation in the interface region make the local electric field increased in the interface region so that the electron quasi-Fermi level could be discontinuous [10,11]. According to Eq. (4), V_{oc} decreases at low temperature due to the increasing local electric field in the interface region.

To further understand the underlying processes relating to the screening effect of the built-in field, the EA measurement was carried out in reverse scan. For the theoretical interpretation of an EA spectrum induced by the Stark effect was first studied in the 1970 s by Liptay [32] and the EA experiments have been recently conducted to investigate the difference in the dipole moment ($\Delta\mu$) and molecular polarizability (Δp) between the excited state and the ground state in the case of perovskite solar cells [13,33–35]. According to the classical Stark effect theory, the shift of the transition energy (ΔE) because of an applied electric field F is obtained from second-order perturbation theory as
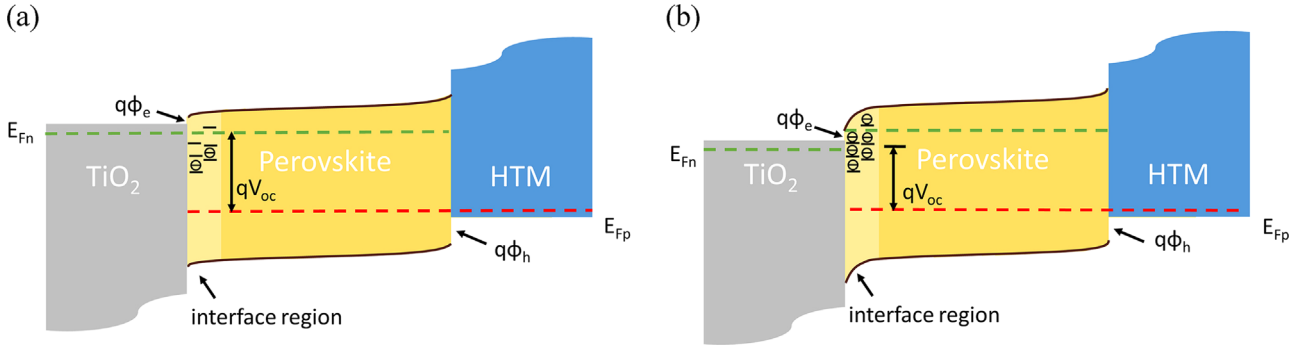
Fig. 7. (a) Band diagram of planar perovskite solar cell above room temperature. (b) Band diagram of planar perovskite solar cell at low temperature. Negative charges accumulating make surface potential of CH$_3$NH$_3$PbI$_3$ increase at the TiO$_2$/CH$_3$NH$_3$PbI$_3$ interface.

$$\Delta E = -\Delta\mu\cdot F - \frac{1}{2}F\cdot\Delta p\cdot F \qquad (5)$$

By Taylor expanding, due to this energy shift and averaging over randomly oriented molecules/dipoles, the change in the absorption coefficient $\Delta\alpha$ or EA signal $\Delta R/R$, as a function of ΔE, can be expressed as [36]

$$\Delta\alpha\infty\frac{\Delta R}{R}\infty\frac{\partial\alpha}{\partial E}\Delta E + \frac{1}{2}\frac{\partial^2\alpha}{\partial E^2}\Delta E^2 \qquad (6)$$

By inserting Eq. (5) into Eq. (6), the EA lineshape can be regarded as a linear combination of the lineshape resembling the first and second derivative of the unperturbed absorption spectrum [34]. If there is no permanent dipole, the whole absorption spectrum will shift towards a lower energy. Thus, the change of absorption $\Delta\alpha$, or the EA spectrum $\Delta R/R$, exhibits a first derivative lineshape. If permanent dipoles exist, $\Delta\mu\cdot F$ dominates Eq. (6). As a result, the EA spectrum resembles a second derivative lineshape.

In a uniform dielectric, the EA response to a sinusoidal voltage of the form $V=V_0+V_{ac}\cos(\omega t)$ is the first-order response at the modulation frequency ω, given as [34,37,38]

$$\Delta\alpha|_\omega\infty\left.\frac{\Delta R}{R}\right|_\omega\infty\chi(h\nu)V_0V_{ac}\sin(\omega t) = \chi(h\nu)(V_{dc} - V_b)V_{ac}\sin(\omega t) \qquad (7)$$

where $\chi(h\nu)$ is related to the complex index of refraction and third order susceptibility of the material as a function of photon energy $(h\nu)$ [39]. V_0 is the internal dc voltage and V_b is the built-in potential in the device. Based on the standard metal–insulator–metal model, the built-in potential V_b relies on the work function difference between two electrodes. By monitoring the EA signal as a function of applied bias, the nulling voltage V_{null} ($V_{null}=V_{dc}-V_b$) can be found when the EA signal is zero. According to Eq. (7), the internal built-in potential V_b across the device can be determined.

As a comparison, we firstly investigated the absorbance spectra, the first-order derivatives of absorbance spectra and the second-order derivatives of absorbance spectra for perovskite film at different temperatures, respectively, as shown in Fig. 8. The absorbance of CH$_3$NH$_3$PbI$_3$ almost remain unchanged over the whole spectrum from 200 K to 325 K, except for the blue shift of the absorption onset. The blue shift is responsible for increasing the bandgap with increasing temperature [12]. In Fig. 9(a), (b), It can be clearly seen that the EA spectral features are well fitted with the second-order derivatives of the absorbance spectra at 275 K and 300 K (Fig. 8(c)), indicating that the second order Stark effect is dominated by the large increase in the electric dipoles ($\Delta\mu$) at the excited states [13]. In Fig. 9(c), the device exhibits a V_b of 0.65 ± 0.05 V at 300 K, whereas this is 0.55 ± 0.05 V at 275 K. The reduction of V_b of 0.1 ± 0.05 V with decreasing operating temperature from 300 K to 275 K, which reflects the red shift of V_{OC} as shown in Fig. 2, could be considered to be the screening effect of
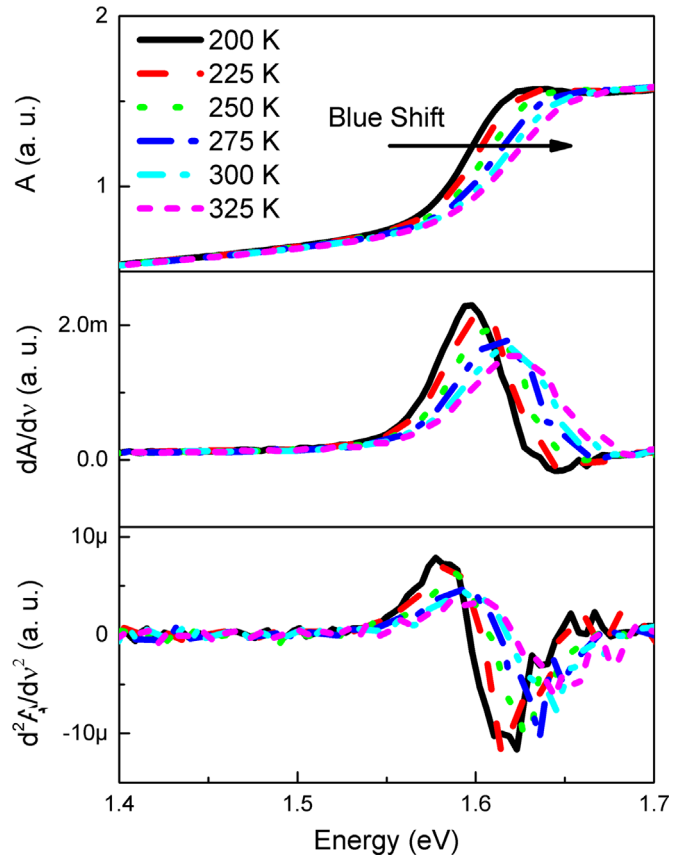

Fig. 8. Absorbance spectra, the first-order derivatives of absorbance spectra and the second-order derivatives of absorbance spectra for perovskite film at different temperatures, respectively.

the built-in field due to a modulation of the interfacial barrier.

As a consequence, for V < Voc condition, the local electric field in the TiO$_2$/CH$_3$NH$_3$PbI$_3$ interface region is enhanced due to the negative charge accumulation, while the built-in field in the absorber layer is reduced. As a result, less electron-hole pairs can be separated and the recombination probability is increased in the absorber layer. The loss of photo-generated carriers leads to the decrease of photo-generated current. To improve the photovoltaic performance of perovskite solar cell, the TiO$_2$/CH$_3$NH$_3$PbI$_3$ interface should be modified carefully, such as passivating the CH$_3$NH$_3$PbI$_3$ surface and increasing the perovskite grain size [30,40].

4. Conclusions

In summary, the temperature dependence of initial transient
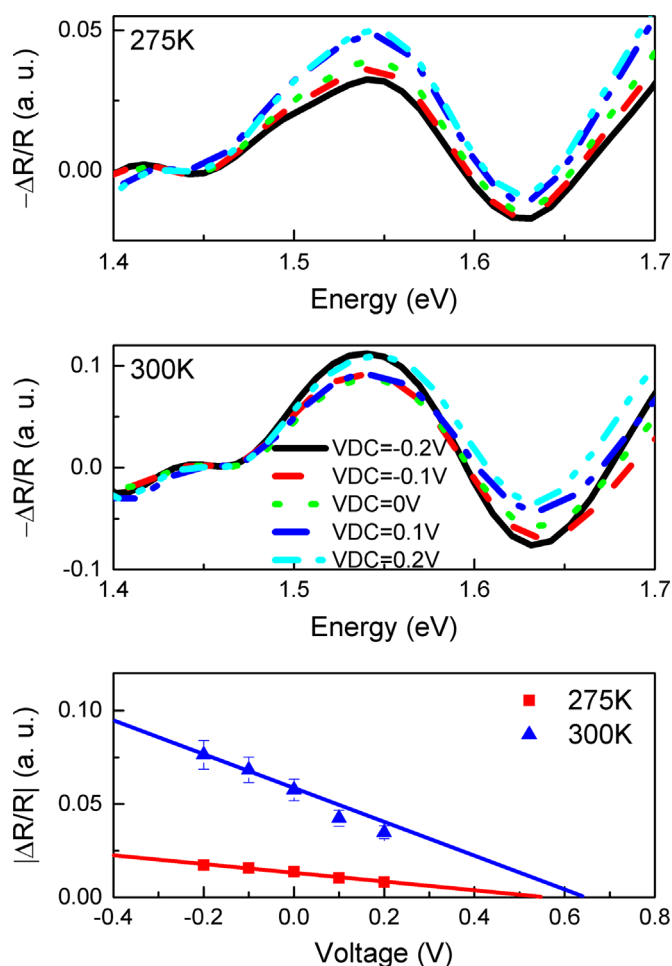
Fig. 9. EA spectra and EA characterization of a perovskite solar cell as function of dc voltages at different temperatures. (a) 275 K, (b) 300 K, (c) dc dependent EA signal at a photon energy of 1.63 eV in reverse mode.

I-V characteristic of planar perovskite solar cell has been studied. With decreasing temperature, the S-shaped I-V characteristic becomes more apparent, meanwhile the photovoltaic parameters continues to decline. The S-shaped I-V curve are fitted by an equivalent circuit model that two opposite parallel diodes are in series with a conventional solar cell model. These two extra diodes represent the influence of negative charges accumulating at trap states and ions in the $TiO_2/CH_3NH_3PbI_3$ interface region on the device. Thus, the electric field is redistributed and the recombination probability of photo-generated carriers increases in the absorber layer. These findings contribute to the understanding of carrier transport mechanism in perovskite solar cell.

Acknowledgements

References

[1] Y. Yamada, T. Nakamura, M. Endo, A. Wakamiya, Y. Kanemitsu, Photoelectronic responses in solution-processed perovskite $CH_3HN_3PbI_3$ solar cells studied by photoluminescence and photoabsorption spectroscopy, IEEE J. Photovolt. 5 (2015) 401–405.

[2] J.H. Im, C.R. Lee, J.W. Lee, S.W. Park, N.G. Park, 6.5% efficient perovskite quantum-dot-sensitized solar cell, Nanoscale 3 (2011) 4088–4093.

[3] A. Kojima, K. Teshima, Y. Shirai, T. Miyasaka, Organometal halide perovskites as visible-light sensitizers for photovoltaic cells, J. Am. Chem. Soc. 131 (2009) 6050–6051.

[4] Research, NREL Cell Efficiency Records (2006) ⟨http://www.nrel.gov/ncpv/images/efficiency_chart.jpg⟩.

[5] H. Zhang, X. Qiao, Y. Shen, T. Moehl, S.M. Zakeeruddin, M. Gratzel, M. Wang, Photovoltaic behaviour of lead methylammonium triiodide perovskite solar cells down to 80 K, J. Mater. Chem A 3 (2015) 11762–11767.

[6] L. Cojocaru, S. Uchida, Y. Sanehira, V. Gonzalez-Pedro, J. Bisquert, J. Nakazaki, T. Kubo, H. Segawa, Temperature effects on the photovoltaic performance of planar structure perovskite solar cells, Chem. Lett. 44 (2015) 1557–1559.

[7] H.J. Snaith, L. Schmidt-Mende, M. Grätzel, M. Chiesa, Light intensity, temperature, and thickness dependence of the open-circuit voltage in solid-state dye-sensitized solar cells, Phys. Rev. B 74 (2006) 045306.

[8] S.R. Cowan, J.V. Li, D.C. Olson, E.L. Ratcliff, Contact-induced mechanisms in organic photovoltaics: a steady-state and transient study, Adv. Energy Mater. 5 (2015) 1400549.

[9] D. Gupta, M. Bag, K.S. Narayan, Correlating reduced fill factor in polymer solar cells to contact effects, Appl Phys. Lett. 92 (2008) 093301.

[10] F.A. de Castro, J. Heier, x Nu, F. esch, R. Hany, Origin of the kink in current-density versus voltage curves and efficiency enhancement of polymer-c60 heterojunction solar cells, IEEE J. Select. Top. Quant. Electron. 16 (2010) 1690–1699.

[11] A. Wagenpfahl, D. Rauh, M. Binder, C. Deibel, V. Dyakonov, S-shaped current-voltage characteristics of organic solar devices, Phys. Rev. B 82 (2010) 115306.

[12] R. Cao, F. Xu, J. Zhu, S. Ge, W. Wang, H. Xu, R. Xu, Y. Wu, Z. Ma, F. Hong, Z. Jiang, Unveiling the low-temperature pseudodegradation of photovoltaic performance in planar perovskite solar cell by optoelectronic observation, Adv. Energy Mater. (2016), http://dx.doi.org/10.1002/aenm.201600814.

[13] X. Wu, H. Yu, L. Li, F. Wang, H. Xu, N. Zhao, Composition-dependent light-induced dipole moment change in organometal halide perovskites, J. Phys. Chem. C. 119 (2015) 1253–1259.

[14] C. Bi, Y. Shao, Y. Yuan, Z. Xiao, C. Wang, Y. Gao, J. Huang, Understanding the formation and evolution of interdiffusion grown organolead halide perovskite thin films by thermal annealing, J. Mater. Chem A 2 (2014) 18508–18514.

[15] C.C. Stoumpos, C.D. Malliakas, M.G. Kanatzidis, Semiconducting tin and lead iodide perovskites with organic cations: phase transitions, high mobilities, and near-infrared photoluminescent properties, Inorg. Chem. 52 (2013) 9019–9038.

[16] A. Naikaew, P. Prajongtat, M.C. Lux-Steiner, M. Arunchaiya, T. Dittrich, Role of phase composition for electronic states in $CH_3NH_3PbI_3$ prepared from $CH_3NH_3I/PbCl_2$ solution, Appl Phys. Lett. 106 (2015) 232104.

[17] F.J. Garcia-Sánchez, D. Lugo-Muñoz, J. Muci, A. Ortiz-Conde, Lumped parameter modeling of organic solar cells's S-shaped I–V characteristics, IEEE J. Photovolt. 3 (2013) 330–335.

[18] W. Li, H. Dong, G. Dong, L. Wang, Hystersis mechanism in perovskite photovoltaic devices and its potential application for multi-bit memory devices, Org. Electron. 26 (2015) 208–212.

[19] G. Xing, B. Wu, S. Chen, J. Chua, N. Yantara, S. Mhaisalkar, N. Mathews, T.C. Sum, Interfacial electron transfer barrier at compact $TiO_2/CH_3NH_3PbI_3$ heterojunction, Small 11 (2015) 3606–3613.

[20] K. Wojciechowski, S.D. Stranks, A. Abate, G. Sadoughi, A. Sadhanala, N. Kopidakis, G. Rumbles, C.-Z. Li, R.H. Friend, A.K.Y. Jen, H.J. Snaith, Heterojunction modification for highly efficient organic–inorganic perovskite solar cells, ACS Nano 8 (2014) 12701–12709.

[21] J. Haruyama, K. Sodeyama, L. Han, Y. Tateyama, First-principles study of ion diffusion in perovskite solar cell sensitizers, J. Am. Chem Soc. 137 (2015) 10048–10051.

[22] Z. Xiao, Y. Yuan, Y. Shao, Q. Wang, Q. Dong, C. Bi, P. Sharma, A. Gruverman, J. Huang, Giant switchable photovoltaic effect in organometal trihalide perovskite devices, Nat. Mater. 14 (2015) 193–198.

[23] D.M. Oman, K.M. Dugan, J.L. Killian, V. Ceekala, C.S. Ferekides, D.L. Morel, Reduction of recombination current in CdTe/CdS solar cells, Appl Phys. Lett. 67 (1995) 1896–1898.

[24] B. Maynard, Q. Long, E.A. Schiff, M. Yang, K. Zhu, R. Kottokkaran, H. Abbas, V.L. Dalal, Electron and hole drift mobility measurements on methylammonium lead iodide perovskite solar cells, Appl. Phys. Lett. 108 (2016) 173505.

[25] R. Varache, C. Leendertz, M.E. Gueunier-Farret, J. Haschke, D. Muñoz, L. Korte, Investigation of selective junctions using a newly developed tunnel current model for solar cell applications, Sol. Energy Mater. Sol. Cells 141 (2015) 14–23.

[26] C. Eames, J.M. Frost, P.R.F. Barnes, B.C. O/'Regan, A. Walsh, M.S. Islam, Ionic transport in hybrid lead iodide perovskite solar cells, Nat. Commun. 6 (2015) 7497.

[27] S. van Reenen, M. Kemerink, H.J. Snaith, Modeling anomalous hysteresis in perovskite solar cells, J. Phys. Chem. Lett. 6 (2015) 3808–3814.

[28] O.J. Sandberg, M. Nyman, R. Österbacka, Effect of contacts in organic bulk heterojunction solar cells, Phys. Rev. Appl. 1 (2014) 024003.

[29] Z. Xiao, Y. Yuan, Y. Shao, Q. Wang, Q. Dong, C. Bi, P. Sharma, A. Gruverman, J. Huang, Giant switchable photovoltaic effect in organometal trihalide perovskite devices, Nat. Mater. 14 (2015) 193–198.

[30] Y. Shao, Z. Xiao, C. Bi, Y. Yuan, J. Huang, Origin and elimination of photocurrent hysteresis by fullerene passivation in $CH_3NH_3PbI_3$ planar heterojunction solar cells, Nat. Commun. 5 (2014) 5784.

[31] D. Cheyns, J. Poortmans, P. Heremans, C. Deibel, S. Verlaak, B.P. Rand, J. Genoe, Analytical model for the open-circuit voltage and its associated resistance in organic planar heterojunction solar cells, Phys. Rev. B 77 (2008) 165332.

[32] W. Liptay, Electrochromism and solvatochromism, Angew. Chem. Int. Ed. 8 (1969) 177–188.

[33] B. Bernardo, D. Cheyns, B. Verreet, R.D. Schaller, B.P. Rand, N.C. Giebink, Delocalization and dielectric screening of charge transfer states in organic photovoltaic cells, Nat. Commun. 5 (2014, http://dx.doi.org/10.1038/ncomms4245).

[34] C. Li, S. Tscheuschner, F. Paulus, P.E. Hopkinson, J. Kießling, A. Köhler, Y. Vaynzof, S. Huettner, Iodine migration and its effect on hysteresis in perovskite solar cells, Adv. Mater. 28 (2016) 2446–2454.

[35] M.E. Ziffer, J.C. Mohammed, D.S. Ginger, Electroabsorption spectroscopy measurements of the exciton binding energy, electron–hole reduced effective mass, and band gap in the perovskite $CH_3NH_3PbI_3$, ACS Photonics 3 (2016) 1060–1068.

[36] L. Sebastian, G. Weiser, H. Bässler, Charge transfer transitions in solid tetracene and pentacene studied by electroabsorption, Chem. Phys. 61 (1981) 125–135.

[37] S. Kazaoui, N. Minami, Y. Tanabe, H.J. Byrne, A. Eilmes, P. Petelenz, Comprehensive analysis of intermolecular charge-transfer excited states in C_{60} and C_{70} films, Phys. Rev. B 58 (1998) 7689–7700.

[38] T.M. Brown, R.H. Friend, I.S. Millard, D.J. Lacey, T. Butler, J.H. Burroughes, F. Cacialli, Electronic line-up in light-emitting diodes with alkali-halide/metal cathodes, J. Appl Phys. 93 (2003) 6159–6172.

[39] I.H. Campbell, T.W. Hagler, D.L. Smith, J.P. Ferraris, Direct measurement of conjugated polymer electronic excitation energies using metal/polymer/metal structures, Phys. Rev. Lett. 76 (1996) 1900–1903.

[40] Y. Yang, Y. Yan, M. Yang, S. Choi, K. Zhu, J.M. Luther, M.C. Beard, Low surface recombination velocity in solution-grown $CH_3NH_3PbBr_3$ perovskite single crystal, Nat. Commun. 6 (2015, http://dx.doi.org/10.1038/ncomms8961).